Remodeling of the core leads HIV-1 pre-integration complex in the nucleus of human lymphocytes.

Guillermo Blanco-Rodriguez, Anastasia Gazi, Blandine Monel, Stella Frabetti, Viviana Scoca, Florian Mueller, Olivier Schwartz, Jacomine Krijnse-Locker, Pierre Charneau, Francesca Di Nunzio

JVI Accepted Manuscript Posted Online 1 April 2020
J. Virol. doi:10.1128/JVI.00135-20

Remodeling of the core leads HIV-1 pre-integration complex in the nucleus of human lymphocytes.

Guillermo Blanco-Rodriguez [1,2], Anastasia Gazi*[3], Blandine Monel*[4], Stella Frabetti*[1], Viviana Scoca*[1], Florian Mueller [5,6], Olivier Schwartz [4], Jacomine Krijnse-Locker [3], Pierre Charneau [1], Francesca Di Nunzio[1#]

[1] *Department of Virology, VMV, 28 rue du Dr. Roux, 75015 Pasteur Institute, Paris, France*
[2] *Ecole Doctorale Frontiere de l'Innovation en Recherche et Education CRI 75004 Paris, Université de Paris 75006 Paris France.*
[3] *Unit for service and technology in ultra-structural bio-imaging, Center for resources and research in technology, 28 rue du Dr. Roux, 75015 Pasteur Institute, Paris, France*
[4] *Department of Virology, UVI, 28 rue du Dr. Roux, 75015 Pasteur Institute, Paris, France*
[5] *Département Biologie Cellulaire et Infections, UIM, 25 rue du Dr. Roux, 75015 Pasteur Institute, Paris, France*
[6] *C3BI, USR 3756 IP CNRS, 28 rue du Docteur Roux; 75015 Paris, France*

* *equal contribution*
[#] *E-mail: dinunzio@pasteur.fr*

Abstract

Retroviral replication proceeds through obligate integration of the viral DNA into the host genome. In particular, HIV-1 genome to enter the nucleus, must be led through the nuclear pore complex (NPC). During HIV-1 cytoplasmic journey, the viral core acts like a shell to protect the viral genetic material from antiviral sensors and ensure an adequate environment for the reverse transcription. However, the relatively narrow size of the nuclear pore channel requires that the HIV-1 core reshapes into a structure that fits the pore. On the other hand, the organization of the viral CA proteins that remain associated to the pre-integration complex (PIC) during and after nuclear translocation is still enigmatic. In this study, we analysed the progressive organizational changes of viral CA proteins within the cytoplasm and the nucleus by immuno-gold labelling. Furthermore, we set up a novel technology, HIV-1 ANCHOR, which enables the specific detection of the retrotranscribed DNA by fluorescence microscopy, thereby offering the opportunity to uncover the architecture of the potential HIV-1 PIC. Thus, we combined the immunoelectron microscopy and ANCHOR technologies to reveal the presence of DNA- and CA-positive complexes by correlated light- and electron microscopy (CLEM). During and after nuclear translocation, HIV-1 appears as a complex of viral DNA decorated by multiple viral CA proteins remodelled in a "pearl necklace" shape. Thus, we could describe how CA proteins reshape around the viral DNA to permit the entrance of the

44 HIV-1 in the nucleus. This particular CA protein complex composed by the integrase and the
45 retrotranscribed DNA leads HIV-1 genome inside the host nucleus.
46 Our findings contribute to the understanding of the early steps of HIV-1 infection and provide
47 new insights into the organization of HIV-1 CA proteins during and after viral nuclear entry.
48 Of note, we are now able to visualize the viral DNA in viral complexes, opening up new
49 perspectives for future studies on viral nuclear fate.
50
51 **Importance**
52 How the reverse transcribed genome reaches the host nucleus remains a main open question
53 related to the infectious cycle of HIV-1. HIV-1 core has a size of ~100 nm, largely exceeding
54 that of the NPC channel (~39 nm). Thus, a rearrangement of the viral CA proteins
55 organization is required to achieve an effective nuclear translocation. The mechanistic of this
56 process remains undefined due to the lack of a technology capable to visualize potential CA
57 sub-complexes in association with the viral DNA in the nucleus of HIV-1-infected cells.
58 By the means of state-of-the-art technologies (HIV-1 ANCHOR system combined with
59 CLEM), our study shows that remodeled viral complexes retain multiple CA proteins but not
60 intact core or only a single CA monomer. These viral CA complexes associated with the
61 retrotranscribed DNA can be observed in the outer and inner side of the NE, and they
62 represent potential PIC.
63 Thus, our study shed light on critical early steps characterizing HIV-1 infection, thereby
64 revealing novel, therapeutically exploitable points of intervention. Furthermore, we developed
65 and provided a powerful tool enabling direct, specific and high-resolution visualization of
66 intracellular and intranuclear HIV-1 subviral structures.
67

68 **Introduction**

69 Upon viral entry, the HIV-1 core is released into the host cell cytoplasm and starts its journey
70 towards the nucleus (1, 2) helped or hampered by cellular factors (3-10). The viral core has a
71 conical shape (120nm x 60nm x 40 nm), composed by ~ 1500 capsid (CA) monomers
72 organized in hexamers or pentamers (11-13). This conical structure acts as a protective shell
73 for the viral DNA against defence mechanisms of the host, like nucleic acid sensors and
74 nucleases (14-16) and can be the target of restriction factors, such as Trim5α and MX2 (9,
75 10). Furthermore, the viral CA seems to participate in two critical steps of HIV-1 life cycle,
76 nuclear translocation (4-7, 17) and integration (18-23). The viral core is considered a fragile
77 structure (24) that could exist only as intact or completely unbundled. However, a recent *in*
78 *vitro* study highlighted the possibility that partial cores can be stabilized by host factors (25).
79 Thus, HIV-1 CA can exist in different forms in infected cells: as intact cores, as monomers,
80 pentamers or hexamers and probably as partial cores. Of note, the viral core largely exceeds
81 the size (11-13) of the nuclear pore channel (26); thus, the core should disassemble before
82 entering the nucleus. The "immediate uncoating" model, which postulates a complete loss of
83 the viral CA proteins (2), has been the most accredited model in the past, supported by the
84 impossibility to co-purify viral CA with other viral proteins at early time points due to its
85 genetic fragility (24, 27). Contrary to this model, Aiken's group (20) was the first to propose a
86 role for CA in post-nuclear entry steps, followed by other studies (21-23, 28). However, the
87 viral CA protein was biochemically detected for the first time in the nucleus of macrophages
88 and HeLa cells by Fassati and colleagues (23). The presence of CA in the nucleus was shown
89 also by the analysis of individual time points of infection in fixed cells using surrogate
90 viruses, or by indirect viral labelling using live imaging (29-38); nonetheless, these studies
91 failed to reveal the organization of CA during viral nuclear translocation. By demonstrating
92 the importance of the CA to regulate and coordinate different steps of HIV-1 life cycle, these
93 findings prompted the development of small molecules (HIV-1 CA inhibitors), thereby
94 promoting the development of a new class of anti-retroviral drugs (39). It should be noted,
95 however, that to date the presence of HIV-1 CA has never been shown in the nucleus of
96 infected primary $CD4^+$ T cells, the main target cells of HIV-1. In addition, the CA-positive
97 structure associated with the reverse transcribed DNA that enters the nucleus, in particular in
98 mitotic cells, remains enigmatic. The details of the morphology of intermediate states of viral
99 replication complexes can be analysed only at the nanometre level, due to their small size
100 (HIV-1 core ~ 100nm)(11). Previous studies showed the possibility to visualize HIV-1 cores

101 in the cytoplasm by CLEM under particular circumstances, such as in the presence of
102 proteasome inhibition (40). Nevertheless, it has been impossible to visualize the intermediate
103 states of viral replication complexes, as well as the organization of the viral PIC during a
104 "quasi" physiological infection at the nanometer level. The viral CA was shown to remain
105 partially associated to the HIV-1 DNA after nuclear entry by confocal microscopy (30). As
106 CA-associated HIV-1 DNA has sub-diffraction size, details on this complex could be revealed
107 only by high resolution imaging, until now unattainable due to the incompatibility of
108 fluorescent DNA labelling techniques, such as DNA FISH or click chemistry (EdU), with
109 transmission electron microscopy (TEM).
110 Our study provides new evidence on the organization of viral CA proteins before, during and
111 after nuclear translocation. To visualize intermediate states of viral replication complexes, we
112 combined CLEM with a novel fluorescent approach to directly label HIV-1 DNA, which we
113 defined HIV-1 ANCHOR. The combination of both technologies, high resolution electron and
114 fluorescence microscopy, highlighted the configuration of the CA protein in viral complexes
115 during the nuclear translocation step. We identified nuclear viral complexes including the
116 crucial components of a potentially functional PIC, the integrase (IN) and the retrotranscribed
117 DNA.
118 We reveal multiple CA proteins in the nucleus of both HeLa cells and primary lymphocytes.
119 We detected in the nuclear side of the NPC, HIV-1 CA complexes organized in a "pearl
120 necklace" shape, according the CA gold distribution, likely, enabling the entry of the viral
121 genome in the host nucleus, the cellular compartment of the viral replication.
122

123 **Results**

124 **Viral reverse transcription correlates with HIV-1 CA and IN association**

125 We analysed the dynamics of the HIV-1 CA and IN association, based on their colocalization,
126 and their link with viral retrotranscription. As the viral IN cannot be efficiently labelled using
127 a direct antibody, we infected HeLa cells with HIV-1 containing a small HA tag fused to the
128 C terminus of the IN (HIV-1ΔEnv IN_{HA} / VSV-G) (41). The genetically modified virus
129 efficiently infected HeLa cells as well as primary $CD4^+$ T lymphocytes similarly to the virus
130 carrying the wild type IN (Fig. 1A, Fig.3B). This feature made this tagged-virus a functional
131 tool to study replication complexes in relation to the structure of the viral capsid. Such HA-
132 labelled IN enabled us to study the association between CA and IN during viral infection
133 using a "quasi" WT virus. Cells fixed at 6 h post-infection showed ~ 60-70% of

134 colocalization of viral CA with the viral IN (Fig. 1A, Fig.1E). Next, we investigated the
135 importance of the presence of CA and IN in cytoplasmic complexes within infected cells for
136 reverse transcription by using a capsid-targeting small molecule, PF74. PF74 binds at the
137 interface between the N-terminal domain (NTD) and the C-terminal domain (CTD) (19, 42)
138 of CA, thus inhibiting HIV-1 infection by blocking nuclear entry in a reportedly bimodal
139 dose-dependent mechanism (19, 42-44). It has been shown that reverse transcription (RT) can
140 occur in the presence of low dose of PF 74 (< 10 μM), while it was impeded at higher doses
141 of this drug (42, 44). We challenged HeLa cells with HIV-1 in the presence or not of PF74,
142 using low (1.25μM) and high (10 μM) doses. Then, we measured IN/CA colocalization spots
143 per cell at 24h post-infection (Fig. 1B) by immunolabelling the viral CA and IN, respectively.
144 When we applied a low dose of PF74, at 24 h post-infection we could detect more CA/IN
145 colocalization (Avg ~20.5 on a total of 595 spots detected) in comparison to the few CA/IN
146 colocalization observed in samples treated with high dose of PF74 (Avg ~ 1.8 on a total of
147 62.9 spots detected) (Fig.1B). In agreement with other studies (19, 44, 45), low dose of PF74
148 allowed for the reverse transcription to occur (~60% with respect to the infected sample
149 untreated with PF74) (Fig. 1C). However, since a low dose of PF74 interferes with the
150 nuclear import of HIV-1, viral replication was not detected in these cells, as reported also by
151 others (Fig. 1C) (19, 44, 45). Instead, control cells (untreated with PF74) allow active viral
152 transcription (Fig. 1B and C). A high dose of PF74 caused a loss of the association between
153 CA and IN, together with a loss of reverse transcription activity (Fig. 1B and C). We
154 corroborated these results by carrying out dose-response experiments to check for the
155 presence of CA/IN cytoplasmic complexes (6 h post-infection) and viral infectivity by beta-
156 gal assay (48h post-infection) (Fig. 1D). These experiments show a progressive loss of viral
157 CA and viral IN association in a dose-response manner to the PF74 drug. Our data indicate
158 that CA/IN association correlates with viral reverse transcription (Fig. 1B, C, D and C).
159

160 **Remodelling of HIV-1 cores.**

161 Next, we sought to visualize in more detail the cytoplasmic structures positive for both CA
162 and IN. We infected HeLa P4R5 cells with 500 ng of p24 per million of cells. The
163 asynchronous HIV-1 infection and the specific time of fixation (6 hours post-infection)
164 allowed visualization of different states of viral replication complexes by EM. We observed
165 several seemingly intact virions residing in endosomes (Fig.2A), consistent with the entry
166 pathway engaged by HIV-1 pseudotyped with VSV-G envelope (46). The intact particles in
167 endosomes contained conical cores, while membrane-free cores, seemingly released from

168 these organelles, were detected in the cytoplasm (Fig. 2A). However, to demonstrate the
169 detection of free cores in the cytoplasm, sections were labelled with anti-CA and a secondary
170 antibody coupled to 10nm gold particles (Fig. 2B). CA-positive viral structures were usually
171 decorated with 2 gold particles (Fig. 2B-ii, -iii), although the viral core is composed by
172 multiple CA monomers. Uninfected cells labelled with anti-CA and a secondary antibody
173 labelled with gold particles revealed only background labelling, showing the specificity of the
174 antibody (Fig. 2B -i). During and after the nuclear viral entry, conical core like structures
175 were not detected and instead the immuno-labelling decorated a different CA-positive pattern
176 (Fig. 2B). On the cytoplasmic side of the nuclear pore we could detect irregular shapes similar
177 to "core like structures" decorated with anti-CA (Fig. 2B -ii, -iii). In the nucleus, however, the
178 same antibody outlined pearl-necklace shapes, composed by multiple CA proteins (Fig. 2B-
179 iv,-v). Cytoplasmic viral complexes were typically decorated by 2 CA gold particles (~ 80%)
180 whereas the nuclear complexes were labelled on average by 3 particles (Fig. 2B). The
181 detection of these particular nuclear CA forms was not antibody dependent, because similar
182 results were obtained with an alternative antibody against CA (AG3.0) (Fig. 2C). Importantly,
183 the difference in gold distribution was also seen with wild-type HIV-1 (Fig. 2D), implying
184 that it did not depend on the route of viral entry. By cryo-EM, we confirmed the presence of
185 multiple CA gold particles forming a "pearl necklace" shape inside the nucleus of infected
186 cells (Fig. 2E). These elongated CA complexes are better resolved by cryo-EM (47) and
187 detected by more gold particles when a protein A coupled to gold was used instead of a
188 secondary antibody (Fig. 2E). This likely related to a better affinity of the protein A for
189 primary antibodies compared to secondary gold-conjugated antibodies. Importantly, different
190 labelling methods highlighted similar structures in the nucleus and confirmed the increase in
191 CA gold labelling in viral complexes after nuclear entry (Fig. 2B, C, D, and E).
192 Taken together, our data indicate that the viral core undergoes a morphological rearrangement
193 during nuclear entry coinciding with an increased CA-labelling by EM likely due to increased
194 accessibility of the antibody.
195
196 **Pearl necklace complexes contain IN and are present in the nucleus of CD4$^+$ T cells**
197
198 The presence of CA gold complexes in the nucleus of HeLa cells suggests that they are part of
199 the viral complexes formed during nuclear translocation. Thus, to further characterize the
200 composition and the spatial distribution of HIV-1 complexes inside and outside the nucleus,
201 we labelled CA and IN with different sizes of colloidal gold conjugates (6 nm and 10 nm,

202 respectively) and imaged them by TEM (Fig. 3A). IN was more frequently associated with
203 intra-nuclear CA structures (Fig. 3A), that were detected by 3 or more CA gold rather than 2
204 CA gold particles. To investigate if these complexes could be observed also in natural HIV-1
205 target cells, we repeated the experiments in primary $CD4^+$ T cells, the natural HIV-1 host
206 cells (Fig. 3B). We observed viral complexes labelled by 2 gold particles in the cytoplasm of
207 $CD4^+$ T cells derived from healthy donors at 9 hours post-infection (Fig. 3C-i). The nuclear
208 CA complexes detected by multiple gold particles were also observed in these cells (Fig. 3C-
209 ii and -iii). Furthermore, the difference between the cytoplasmic and nuclear CA gold
210 labelling was similar in HeLa cells and in primary lymphocytes (Fig.2B and 3D).
211 Our results show that viral CA complexes associated with viral IN can be found in the
212 nucleus of HeLa cells, and also in that of natural HIV-1 target cells, i.e. primary lymphocytes.
213 Thus, the formation of the CA nuclear complexes was not cell dependent, implying that they
214 represent an important feature for the nuclear journey of HIV-1.
215
216 **Specific detection of retrotranscribed DNA in infected cells by HIV-1 ANCHOR system.**
217 To investigate if the observed CA structures, detected during and after nuclear translocation,
218 represent potential PICs, we analysed whether the retrotranscribed viral genome was present
219 in these complexes. The rarity of viral events during nuclear import made their visualization
220 particularly difficult. Labelling of the retrotranscribed viral DNA has been a major challenge
221 and only partial success has been achieved using DNA FISH, View HIV assay, multiplex
222 immunofluorescent cell-based detection of DNA, RNA and Protein (MICDDRP), or EdU in
223 fixed cells (18, 29-31, 48-51). These DNA fluorescent labeling methods are all incompatible
224 with TEM technique. This limitation impeded the characterization of the PIC during nuclear
225 translocation. To overcome this drawback, we set up a new system that allowed direct
226 tracking of viral retrotranscribed DNA in CA-positive complexes. We adapted ANCHOR
227 technology (NeoVirTech) (52, 53) to visualize HIV-1 DNA (Fig. 4A). The ANCHOR
228 technology consists in a bipartite system derived from a bacterial parABS chromosome
229 segregation machinery. This is composed by a target DNA sequence, ANCH3, which is
230 specifically recognized by the OR protein, a modified version of the bacterial parB protein
231 (54, 55), fused to GFP. We cloned ANCH3 sequence in the HIV-1 genome (HIV-1 ANCH3)
232 to ensure direct labelling of the retrotranscribed viral DNA in a highly specific manner (the
233 human genome of the host cells lacks the ANCH3 sequences).We used this virus to infect
234 HeLa cells previously transduced with a LV carrying OR-GFP cDNA (LV OR-GFP) (Fig. 4A
235 and B). Our results by fluorescence microscopy revealed that HIV-1 ANCH3 is recognized by

236 OR-GFP fusion proteins that accumulated on the target sequence resulting in the formation of
237 a bright fluorescent spot (Fig. 4B). OR-GFP protein has no nuclear localization sequence
238 (NLS) and therefore freely diffuses in the cell, with predominant localization in the cytoplasm
239 (53). Upon infection, OR-GFP was efficiently visualized in complex with the retrotranscribed
240 viral DNA, particularly in the nucleus (Fig. 4B). Of note, cells infected with HIV-1 ANCH3
241 or with the untagged HIV-1 showed similar number of proviruses by Alu PCR, thus both
242 viruses behaved similarly during integration or steps of infection prior to integration (Fig.
243 4B). Importantly, HIV-1 ANCHOR permitted to track HIV-1 DNA by live-cell imaging.
244 Hence, we could follow the fate of the viral DNA from the reverse transcription step onward.
245 Indeed, this technology enabled us to follow the HIV-1 DNA for more than 70h in living cells
246 by epifluorescence (Suppl. movies 1A,B), or by 3D or 2D spinning disk microscopy (suppl.
247 movies 2A,B,C). Via the latter, we imaged infected cells to obtain complete information
248 about the full cellular volumes. Next, to pinpoint the specificity of HIV-1 ANCHOR system
249 to detect exclusively HIV-1 DNA, we infected HeLa OR-GFP cells with different MOIs
250 (multiplicity of infection) of HIV-1 ANCH3. We observed a linear correlation between MOI
251 and the number of nuclear vDNA spots in GFP+ infected cells (Pearson's coefficient ~ 1)
252 (Fig.5A). The total number of intranuclear spots analysed for each condition was 2054 counts
253 for 34 GFP+ infected cells (MOI 200), 393 counts for 38 GFP+ cells (MOI 30), 290 counts
254 for 44 GFP+ cells (MOI 10). Averages (Avg) of nuclear spots were calculated for single
255 condition (MOI 10 Avg 6.7; MOI 30 Avg 10.07; MOI 200 Avg 60.4) (Fig. 5A). In addition,
256 we infected cells in the presence of drugs, PF74 or nevirapine (NEV, inhibitor of RT). First
257 we challenged HeLa cells expressing OR-GFP with HIV-1 ANCH3 for 24h without drug or
258 in the presence of low and high doses of PF74 (Fig.5B and C). Both doses of PF74 blocked
259 viral nuclear entry (Fig. 5D) (44). We detected the viral DNA inside the nucleus mainly in the
260 absence of PF74 (Fig. 5B and C; suppl. movies 3A,B,C), in agreement with nuclear import
261 data obtained by qPCR (Fig. 5D). Total intranuclear spots were analysed for each condition
262 (no drugs 180 spots in 13 GFP+ cells; PF74 low dose 8 spots in 28 GFP+ cells; PF74 high
263 dose 1 spot in 27 GFP+ cells) (Fig. 5C). These results were confirmed also when the
264 nevirapine was used. We counted intranuclear spots in 20 cells per condition and we obtained
265 the following results: 152 nuclear spots in absence of NEV against 0 detections in presence of
266 the drug. Thus, nuclear punctae containing HIV-1 DNA were found only in NEV untreated
267 cells (Fig. 5E; suppl. movies 4 A,B). Overall, these observations demonstrated that HIV-1
268 ANCHOR technology faithfully tracked the retrotranscribed viral DNA.
269

HIV-1 CA decorates the retrotranscribed viral DNA during nuclear translocation.

Our ultimate goal was to characterize the CA- and vDNA-positive complexes during and after nuclear translocation. One of the advantages of the OR-GFP system is its compatibility with TEM. Since this system is based on the interaction of OR protein with the ANCH3 sequence we were able to apply a correlative light and electron microscopy approach. Thus, we coupled HIV-1 ANCHOR to immunogold labelling to investigate if the viral DNA was part of the "pearl necklace" CA shapes previously detected by TEM (Fig. 2B-iv,-v; 2C, D and E; 3A and C-ii,-iii). We transduced HeLa cells with LV OR-GFP and 3 days later we challenged those cells with HIV-1 ANCH3 for 6 hours. Cells were fixed and prepared for EM-immuno-labelling to test if structures positive for CA also contained viral DNA. Hence, we observed HIV-1 CA complexes near the nuclear pore complex (NPC) at 6h post infection. These CA complexes were positive for DNA as observed by the correlative method (Fig. 6A). CA-positive complexes typically decorated by 3 CA gold particles, were also associated with HIV-1 DNA during nuclear translocation (Fig. 6B). The error of correlation between the two images (EM and fluorescence) has been calculated by ecCLEM plugin on Icy software (56, 57) to be theoretically ~ 70nm. CLEM results show a more elongated CA-positive form associated to the viral DNA during nuclear translocation (Fig. 6B) than the CA- DNA-positive complex observed in the cytoplasm near the NE (Fig. 6A). These results imply that this form of a viral complex can fit the size of the NPC and translocate through the pore to reach the host nuclear environment. Additionally, we performed a dual gold labelling experiment to detect viral complexes in the nucleus. We used different size of gold particles to label the viral DNA through OR-GFP (anti-GFP, 5 nm gold) and the viral CA (10 nm gold). Interestingly we detected multiple gold particles labelling the viral DNA (5 nm) associated with CA (10 nm) adopting a linear configuration at the NE (Fig.7A). This morphology corroborated the form of the PIC detected by CLEM (Fig. 6B). We were also able to reveal complexes formed by the viral DNA associated to HIV-1 CA in the nucleus of infected dividing cells (Fig. 7B). These data are in line with our CLEM results, showing that viral complexes containing the retrotranscribed DNA can retain several CA proteins even after nuclear translocation.

Overall results obtained by TEM and by CLEM highlighted the shape of a potential HIV-1 PIC during and after the nuclear entry step. Importantly the detected viral complexes contain all required components for the integration, such as the integrase, DNA and, surprisingly, multiple CA proteins.

304 **Discussion**

313 HIV-1 core must undergo structural changes to be able to cross the NPC, as the pore is too
314 narrow to allow its passage as an intact core. Thus, the organization of viral CA complexes
315 during the early steps of HIV-1 infection is still unknown, due to the lack of appropriate tools
316 to study this event. Our study provides some new evidences on the viral remodelling of HIV-
317 1 core occurring prior, during and after viral nuclear entry. Importantly we confirmed such
318 observation in the main physiological target cell of HIV-1, CD4+ T cells. We were able to
319 quantify a different distribution of CA gold labelling by comparing cytoplasmic and nuclear
320 structures (Fig. 2B), supporting a viral CA remodelling process during nuclear entry. We
321 observed that multilobe structures resembling to "core like shapes" can be labelled by 2 gold
322 particles, although the HIV-1 core is composed by ~1500 CA monomers (12, 58). This can be
323 explained by specific features of EM immuno-labelling that is dependent on the specificity of
324 the antibody, accessibility and number of antigens on thin sections, amongst other factors
325 (59). Intranuclear CA complexes were detected by more gold particles than the cytoplasmic
326 viral structures, which we believe is due to rearrangement of the viral CA (Fig. 2B-iv,-v, C, D
327 and E). It should be noted that so far the presence of multiple CA proteins inside the nucleus
328 of infected mitotic cells has never been reported. To confirm the detection of intranuclear
329 complexes, tomograms performed at 6 hours post infection revealed the formation of pearl
330 necklace shapes composed by multiple CA located in the nucleus (Fig. 2E). Often these
331 nuclear CA structures are associated to viral IN (Fig. 3A). Importantly, similar complexes
332 composed by multiple CA and IN have been identified in HeLa cells and primary
333 lymphocytes, revealing the organization of the viral CA proteins also in the main target cells
334 of HIV-1 (Fig. 3C). Our results show that viral complexes observed during nuclear
335 translocation could represent PICs, thanks to the ability to combine the specific labelling of
336 the retrotranscribed DNA (HIV-1 ANCHOR) with immunogold CA labelling. So far the viral
337 DNA has never been visualized associated to multiple CA proteins in dividing infected cells.
338 Importantly, we observed that HIV-1 ANCHOR allowed the specific detection of the viral
339 DNA as shown by the use of drugs (Fig. 5). This is highlighted by using drugs that block
340 different steps of the HIV-1 early events, such as nuclear import (PF74 drug) or reverse
341 transcription (nevirapine) (Fig 5). Bright spots identifying viral DNA were prevalently
342 detected in the nucleus of untreated cells, in agreement with results obtained by real time PCR
343 that amplified 2LTR circles (Fig. 5B, C and D), commonly used to detect viral nuclear import
344 (60). Thus, CLEM enabled to visualize the organization of HIV-1 PIC during nuclear
345 translocation in HIV-1-permissive cells. It should be noted that HIV-1 ANCHOR can

346 specifically label all nuclear viral DNA forms, thus, further experiments are needed to
347 distinguish integration competent viral complexes from dead-end products. Independently of
348 the fate of the PIC, HIV-1 ANCHOR technology combined with EM offered the opportunity
349 to observe how viral CA proteins reshape near the NPC to lead the viral genome in the
350 nucleus (Fig. 6A and B). OR-GFP can bind the viral DNA only if it is exposed, as indicated
351 by our CLEM results, which support our model of viral core remodelling. In fact, complexes
352 of multiple CA associated to the retrotranscribed DNA can be visualized by CLEM before
353 and during the nuclear translocation (Fig. 6A and B). Likely, the observed complexes contain
354 complete retrotranscribed genomes. In agreement with this observation, previous studies
355 showed that OR-GFP binds only dsDNA (61), meaning that the vDNA shrouded in the
356 multiple CA proteins complex is a dsDNA. The ANCH3 sequence has been cloned in nef
357 gene, which means that the vDNA identified by CLEM might be a late reverse transcript,
358 since OR-GFP can only bind it after the completion of reverse transcription on both strands
359 containing the ANCH3 sequence. Thus, all viral complexes carrying an accessible vDNA can
360 be observed by fluorescence microscopy. As opposed to fluorescence microscopy, the
361 visualization of viral complexes by EM coupled with gold labeling is more complicated, but
362 has the advantage of yielding high resolution images. Sections are not permeabilized, so only
363 CA epitopes exposed on the surface of the section can be labeled by the anti-CA antibody and
364 then by a secondary gold labeled antibody. Indeed, a limited number of available epitopes can
365 be recognized by the primary antibody in sections. The aforementioned reasons, together with
366 the thorough sample fixation required for the EM strictly limit the number of epitopes
367 accessible to the antibody, therefore we observed more vDNA signal than CA protein signals.
368 Apart from such technical limitations, we do not expect to have all vDNA complexes co-
369 labeled with CA, as a result of the asynchronous infection conditions used and the consequent
370 presence of some CA-free nuclear vDNA, as previously shown by Brass group (30). On the
371 other hand, most of the HIV-1 particles are known to undergo an abortive uncoating in the
372 cytoplasm. Thus, we focused to those viral CA complexes that contain also the vDNA,
373 interestingly, these viral complexes were found in the vicinity of the NE. Overall, these
374 results indicate that the viral complexes visualized by CLEM could potentially be PICs.
375 Summarizing, the viral CA reshapes before crossing the NPC, decorating the viral DNA and
376 leading it into the nucleus. Similar CA-viral DNA complexes can be also found near the NE
377 (Fig. 7A) and inside the host nuclei (Fig. 7B).
378 The presence of consistent shapes formed by multiple CA proteins in the nucleus (Fig. 2B-iv,-
379 v, C, D and E; Fig. 3A and C), as well as their association to the retrotranscribed DNA (Fig.

380 6A and B; Fig. 7A and B), would indicate that these CA forms are imported with the viral
381 genome into the host nucleus. These results would support the evolution of the concept of
382 viral uncoating, no more seen as a complete loss of viral CA but as a CA remodelling during
383 nuclear import. Another novel aspect of our work is the development of the HIV-1
384 ANCHOR system, the first fluorescence DNA labelling technique shown to be compatible
385 with TEM. This innovative technology allows us to follow the HIV-1 DNA shrouded by
386 multiple CA proteins during and after nuclear entry in mitotic cells. In addition, we were able
387 to live-track the viral DNA in the nucleus of infected cells following translocation through the
388 pore (suppl. movies 1,2,3,4).
389 Of note, our study gives new information on the early steps of HIV-1 infection in dividing
390 cells. It is known that mitotic cells with integrated viruses may persist for many years,
391 undergo clonal expansion (62). Clonal expansion seems to be the major mechanism to
392 generate HIV-1 reservoir (63), considered to be established early during primary HIV-1
393 infection (64).
394 Overall, our results provide new notions not only on the organization of viral PIC complexes
395 but also on the dynamics and the fate of the viral DNA inside the nucleus. Our data elucidate
396 how the viral CA remodels to lead HIV-1 DNA in the nucleus of infected cells.
397
398 These findings and technology can be useful for future studies on other pathogens or to
399 investigate the interplay of HIV-1 DNA with nuclear factors and chromatin environments.
400
401

402 **Methods**
403
404
405 **Cells.** HeLaP4R5 cells, a HeLa-CD4/LTR-lacZ indicator cell line expressing both CXCR4
406 and CCR5, were employed to assess viral infectivity (65) using a beta gal assay. 293T cells
407 (ATCC) are human embryonic kidney cells used to produce lentiviral vectors and HIV-1
408 viruses, HeLa cells (ATCC) derived from cervical cancer cells. $CD4^+$ T cells were isolated
409 from healthy donors obtained via the EFS (Etablissement Français du Sang, Paris, France).
410 Briefly, primary $CD4^+$ T cells were purified from human peripheral blood by density gradient
411 centrifugation (Lymphocytes separation medium, PAA) followed by positive
412 immunomagnetic selection with CD4 Microbeads (Miltenyi). The day later cells were
413 activated by T Cell Activation kit (Miltenyi) for 2-3 days at 37°C with interleukin 2 (IL-2)-
414 containing medium (50 IU/ml), then cells were challenged with HIV-1 carrying the CA wild
415 type or mutated. Percentage of p24 positive cells has been obtained cytofluorimetry
416 acquisition and FlowJo analysis.
417
418 **Antibodies.** Ab anti- actin HRP conjugated sc-2357 Santa Cruz (dil. 1:5000), Ab anti-p24
419 antibody NIH183-H12-5C or AG3.0 (NIH reagent, IF dil. 1:400 or TEM 1:50) and the anti-
420 HA high affinity antibody (11867423001) Roche (TEM 1:50 dilution or IF 1:500), Ab Goat
421 anti-mouse Alexa Fluor Plus 488 (A32723) and Goat anti-rat Alexa 647 (A21247)
422 Thermofisher scientific. Ab Goat anti-mouse 10nm gold coupled (ab39619), Ab Goat anti-rat
423 6nm gold coupled (ab105300) Abcam (dil. 1:50), Ab Goat anti-rabbit coupled to 5nm gold
424 Abcam (ab27235). Ab anti-GFP rabbit (ab183734) Abcam (CLEM dil. 1:50), Ab anti-GFP
425 (Clontech #632592, WB dilution 1:1000), Ab Beta Actin HRP conjugated (Abcam, #8226
426 WB dil. 1:2,500), Ab Goat anti-rabbit Alexa 488 (A11078) (CLEM dil.1:50), Ab anti Nup153
427 9 (kind gift from B. Burke dil. 1:200), Protein A-10 nm gold (dil. 1:50) from UMC-Utrecht,
428 Netherlands

429 **Time-lapse microscopy.** HeLaP4R5 cells stably transduced with LV OR-GFP were plated in
430 Hi-Q4 microdishes (10,000 cells per chamber) (Ibidi). The following day, cells were infected
431 with HIV-1ΔEnvIN$_{HA}$ΔNefANCH3/VSV-G. Transmission and fluorescence images were
432 taken every 5 or 10 min for up to 96 h using a Nikon Biostation IMQ (40X objective) with 6-
433 8 fields captured simultaneously for each condition or for up to 24h by using a spinning-disk
434 UltraView VOX (Perkin-Elmer) (63x objective) with one field of view for each experiment
435 in 2D or 3D. Images were analyzed in FIJI or Imaris.

436 **Western blotting and confocal immunoimmunofluorescence microscopy.** The correct
437 expression of OR-GFP after LV transduction has been evaluated in HeLa cells by western
438 blotting. Proteins were extracted on ice from wild type and LVOR-GFP transduced HeLa
439 cells using RIPA buffer (20mM HEPES pH 7.6, 150mM NaCl, 1% sodium deoxycholate, 1%
440 Nonidet P-40, 0.1% SDS, 2mM EDTA, complete protease inhibitor (Roche Diagnostics)),
441 and protein concentration was quantified using the Dc Protein Assay (Bio-Rad Laboratories)
442 with BSA as standard. Ten micrograms of total protein lysate was loaded onto SDS–PAGE 4–
443 12% Bis Tris gels (Invitrogen). Revelation was carried out using the ECL Plus western
444 blotting kit (GE Healthcare). Primary antibody used for western blotting (WB) was anti-GFP
445 (Clontech #632592, dilution 1:1000). Secondary conjugated antibodies used for western
446 blotting were Beta Actin HRP conjugated antibody (Abcam, #8226 1:2,500), and anti-rabbit
447 IgG HRP (sc2357 Santa Cruz). Immunofluorescence microscopy: HeLa P4R5 cells stably
448 expressing OR-GFP or not were plated onto 12 mm diameter coverslips in 24-well plates the
449 day before and then infected with HIV-1ΔEnvIN$_{HA}$ΔNef ANCH3/VSV-G or HIV-
450 1ΔEnvIN$_{HA}$ /VSV-G at different MOIs and different time post infection. The cells were then
451 washed, fixed with 4% PFA, permeabilized with Triton X-100 0.5% for 30 min and blocked
452 with 0.3% bovine serum albumin (BSA). All incubations were carried out at room
453 temperature and were followed by five PBS washes. Cells were incubated with primary
454 antibodies for 1 h and secondary antibodies for 30 min. Antibodies were diluted in 0.3%
455 BSA. Nuclei were stained with Hoechst (Invitrogen, dilution 1:10000). Finally, cells were
456 mounted onto glass slides (Thermo Scientific) with Prolong Diamond (Life Technologies).
457 Confocal microscopy was carried out on a Zeiss LSM700 using a 63× objective.
458 Representative medial sections or combined Z-stacks are shown as indicated. Images were
459 analyzed in FIJI.

460

461 **Viral infection and sample preparation for electron microscopy.** Eight million of HeLa
462 P4R5 or Hela P4R5 OR-GFP transduced cells were seeded in a T75 flask and infected with
463 4000ng of p24 of either HIV-1 IN-HA or HIV-1 ANCH3 and incubated for 6h. When a WT
464 virus has been used to infect HeLa P4R5 cells or primary CD4^{+} T cells a ultracentrifuged
465 virus has been used in some cases in presence of SEVI according a published protocol (66,
466 67) (SEVI fibrils have been kindly provided by Franck Kirchhoff). Infectivity has been
467 analysed by beta gal assay or by FACS. Samples were prepared for EM as follows: cells were
468 fixed by adding directly an equal volume of 8% paraformaldehyde, 0.2% glutaraldehyde in

469 PHEM buffer (60mM Pipes, 25mM Hepes, 2mM $MgCl_2$, 10mM EGTA, pH 7.3) solution to
470 the cells medium and incubated for 30 minutes. Next, the solution was exchanged by 4%
471 paraformaldehyde diluted in PHEM buffer and incubated for 2 hours at room temperature.
472 Cells were further prepared for cryomicrotomy and immunolabelled as described in(68).
473 Electron microscopy chemicals were purchased from Electron Microscopy Sciences
474 (Pennsylvania). For the CLEM experiments before contrasting with uranyl acetate the
475 samples were stained with Hoechst 1µM for 20 minutes in water, washed and incubated with
476 a solution of 0.2µm Tetraspeck fluorescent beads (Thermofisher scientific) diluted 1:50 in
477 PHEM buffer pH 7.3 for 20 minutes and washed 4 times 2 minutes with water. The samples
478 were mounted on in a glass bottom petri dish (Miltenyi Biotec) with a drop of SlowFade
479 Diamond antifade mountant (Thermofisher Scientific). The imaging process gave a mosaic
480 map of the sections in the blue, green and far red channels using a 63X 1.4 NA objective with
481 a Leica DSM6000 microscope equipped with Orca Flash 4.0 LT camera (Hamamatsu
482 Photonics). Then the grids were recovered by pouring 10ul of water underneath them. Grids
483 were washed contrasted and prepared for TEM as specified above. For the cryo-EM
484 observation the samples were prepared as described above. After immunolabelling the grids
485 were embedded with a mixture of 50% methylcellulose 2% and 50% sucrose 2.3M and then
486 vitrified by plunge freezing with EMGP plunge freezer (Leica) at 30 °C and 90% humidity.

487

488 **Electron microscopy data collection and image processing.** Sections, at room temperature
489 or in cryo, were transferred and imaged in a Tecnai T12 transmission EM operating at 120 or
490 80kV equipped with a Gatan Ultrascan 4000 camera. Multiscale mapping and tilt series
491 acquisitions in areas of interest were processed by a Serial EM software(69). In case of cryo
492 samples, low dose conditions and bi-directional tilt schemes were used during acquisition.
493 Tilt series stacks were initially aligned using cross-correlation and the alignments were further
494 refined using the immunogold beads as registration fiducials in IMOD (70). Tomograms were
495 reconstructed with the weighted back-projection method and filtered to assist manual
496 segmentation with IMOD.
497 The correlation between fluorescence and electron microscopy were achieved using the
498 following protocol: 1) z-stacks of every frame of the mosaic was projected with the FIJI's
499 plugin extended depth of field(71); 2) the frames were aligned and blended to generate a
500 fluorescence map of the complete section using Mosaic J (72); 3) the same cells was
501 identified in both fluorescence and low resolution TEM section map; 4) the high precision

502 correlation was obtained by identifying Tetraspecks positions in high resolution fluorescence
503 and TEM images using ec-CLEM plugin (57) of Icy (56).).
504
505 **Quantitative PCR.** Total cellular DNA was isolated using the QIAamp DNA micro kit
506 (QIAGEN) at 7 and 24 h post infection. The genomic DNA was treated for 1h at 37 ºC with
507 Dpn1. Ten micromolar of nevirapine was used in infected cells as control of the experiment.
508 Late reverse transcription products at 7 h post infection were measured by real-time PCR
509 using primers and probe previously described (60), 2LTR containing circles were detected
510 using primers MH535/536 and probe MH603, using as standard curve the pUC2LTR plasmid,
511 which contains the HIV-1 2LTR junction. Integration was assessed by Alu-PCR, using
512 primers designed in the U3 region of LTR (4) which is deleted in the LVs carrying OR-GFP
513 but not in the LTR of HIV-1 used to challenge OR-GFP stably expressing cells and control
514 cells. The standard curve has been prepared as follows: DNA generated from infected cells
515 was end point diluted in DNA prepared from uninfected cells and serial dilutions were made
516 starting from 50,000 infected cells. Each sample amplified contained 10,000 infected cells
517 mixed at 40,000 uninfected cells. The control of the first round PCR was the amplification
518 without Alu primers but only U3 primers (4). Dilutions 1:10 of the first round were amplified
519 by real time PCR (4). Internal controls have been included such as infection in presence of
520 RAL (10µM). LRT, 2-LTR and Alu-PCR reactions were normalized by amplification of the
521 housekeeping gene Actin (4).
522
523 **Plasmids and viral production.** HIV-1ΔEnvIN$_{HA}$ΔNef ANCH3 plasmid was obtained by
524 PCR using as template the plasmid pANCH3 (NeoVirTech, NVT)(53). Primers containing the
525 restriction site for XhoI have been applied to amplify ANCH3 sequence (~1Kb). The
526 amplicon has been cloned in XhoI site of HIV-1ΔEnvIN$_{HA}$. The final plasmid HIV-
527 1ΔEnvIN$_{HA}$ΔNef ANCH3 has been sequenced. The LVCMVOR-GFP was generated by
528 cloning by PCR OR-GFP from the plasmid pOR-GFP (NeoVirTech)(53) in pTripCMVGFP.
529 We amplified OR-GFP (~1.8Kb) using specific primers to amplify the cDNA OR-GFP
530 (NeoVirTech property), the primers, named OR-GFP 5' and OR-GFP 3' used contain
531 restriction sites for AgeI and SgrDI to allow the cloning in pTripCMVGFP. The resulted
532 plasmids has been accurately sequenced and compared with ANCH3 and OR-GFP sequences
533 from respective plasmids obtained by NeoVirTech. The ANCHOR^{TM} technology is the
534 exclusive property of NVT. Lentiviral vectors and HIV-1 viruses were produced by transient
535 transfection of 293T cells using calcium phosphate coprecipitation. Lentiviral vectors were

536 produced by co-transfection of 10 µg of transfer vector LV OR-GFP with 2.5 µg of pMD2
537 VSV-G and 10 µg of ΔR8.74 plasmids. HIV-1 viruses were produced by cotransfection with
538 calcium phosphate with HIV-1 LAI (BRU) ΔEnv Virus (NIH) or with the modified versions
539 HIV-1ΔEnvIN$_{HA}$ (41) (kindly provided by Fabrizio Mammano) or HIV-1ΔEnvIN$_{HA}$ΔNef
540 ANCH3 and VSV-G envelope expression plasmid pHCMV-G (VSV-G). The viruses
541 collected from 293T cells 48 h post transfection were ultracentrifuged at 4 ºC for 1h at 22,000
542 rpm. Virus normalizations were performed by p24 ELISA according to the manufacturer's
543 instructions (Perkin Elmer) and by real time PCR. The titer of each virus has been calculated
544 by qPCR as transducing unit (TU)/mL and then used to calculate the MOI (TU / number of
545 cells). Infectivity has been tested by Beta-galactosidase assay (Merck) activity measured 48 h
546 post infection according to manufacturer's instructions, using a microplate fluorimeter
547 (Victor, Perkin Elmer). Protein quantification by Bio-Rad protein assay was carried out on the
548 same lysates to normalize the B-gal data for protein content.
549
550
551 **Acknowledgements**

552 We wish to thank Philippe Souque, François Anna and Olivier Gourgette for experimental
553 help, Fabrizio Mammano, Nicoletta Casartelli and Franck Gallardo for scientific discussion
554 and critical reads of the manuscript. We thank Daniela Bruni for help editing the manuscript.
555 We thank Sylvie van der Werf and the department of Virology IP to support the end of the
556 contract of G.B.-R. We thank Fabrizio Mammano, Franck Kirchhoff and NIH reagents
557 program for sharing reagents. Julie Ravel for the inspiration of the study. We thank the
558 members of the Imagopole Platform at the IP. We thank the NIH AIDS Reagents program to
559 support us with precious reagents. This work was funded by the ANRS (Agence Nationale de
560 Recherche sur le SIDA) grant ECTZ4469, the Sidaction/FRM grant n.11291, the Pasteur
561 Institute.
562
563
564
565 **Author contributions**

566 F.D.N. conceived the study. G.B.-R. and F.D.N. designed the experiments and wrote the
567 manuscript. B.M. and F.D.N. performed live imaging experiments. F.D.N. conceived the
568 HIV-1 ANCHOR system. G.B-R., A.G., F.D.N. and J.K.-L. designed electron microscopy
569 experiments, G.B-R. and A.G. conducted electron microscopy experiments and analysed data.
570 G.B-R. set up and analysed CLEM using immunogold labelling and HIV-1 ANCHOR
571 system. G.B.-R. and F.D.N. performed IF experiments. V.S. performed qPCR experiments
572 and S.F. conducted western blotting, molecular cloning and viral productions. G.B.-R., V.S.

and F.D.N. analysed imaging data. F.M., J.K.-L., O.S. and P.C. contributed to stimulating discussions.

Competing financial interests: The authors declare no competing financial interests.

References

1. McDonald D, Vodicka MA, Lucero G, Svitkina TM, Borisy GG, Emerman M, Hope TJ. 2002. Visualization of the intracellular behavior of HIV in living cells. J Cell Biol 159:441-52.
2. Campbell EM, Hope TJ. 2015. HIV-1 capsid: the multifaceted key player in HIV-1 infection. Nat Rev Microbiol 13:471-83.
3. Lelek M, Casartelli N, Pellin D, Rizzi E, Souque P, Severgnini M, Di Serio C, Fricke T, Diaz-Griffero F, Zimmer C, Charneau P, Di Nunzio F. 2015. Chromatin organization at the nuclear pore favours HIV replication. Nat Commun 6:6483.
4. Di Nunzio F, Fricke T, Miccio A, Valle-Casuso JC, Perez P, Souque P, Rizzi E, Severgnini M, Mavilio F, Charneau P, Diaz-Griffero F. 2013. Nup153 and Nup98 bind the HIV-1 core and contribute to the early steps of HIV-1 replication. Virology 440:8-18.
5. Di Nunzio F, Danckaert A, Fricke T, Perez P, Fernandez J, Perret E, Roux P, Shorte S, Charneau P, Diaz-Griffero F, Arhel NJ. 2012. Human nucleoporins promote HIV-1 docking at the nuclear pore, nuclear import and integration. PLoS One 7:e46037.
6. Matreyek KA, Yucel SS, Li X, Engelman A. 2013. Nucleoporin NUP153 phenylalanine-glycine motifs engage a common binding pocket within the HIV-1 capsid protein to mediate lentiviral infectivity. PLoS Pathog 9:e1003693.
7. Schaller T, Ocwieja KE, Rasaiyaah J, Price AJ, Brady TL, Roth SL, Hue S, Fletcher AJ, Lee K, KewalRamani VN, Noursadeghi M, Jenner RG, James LC, Bushman FD, Towers GJ. 2011. HIV-1 capsid-cyclophilin interactions determine nuclear import pathway, integration targeting and replication efficiency. PLoS Pathog 7:e1002439.
8. Lee K, Ambrose Z, Martin TD, Oztop I, Mulky A, Julias JG, Vandegraaff N, Baumann JG, Wang R, Yuen W, Takemura T, Shelton K, Taniuchi I, Li Y, Sodroski J, Littman DR, Coffin JM, Hughes SH, Unutmaz D, Engelman A, KewalRamani VN. 2010. Flexible use of nuclear import pathways by HIV-1. Cell Host Microbe 7:221-33.
9. Stremlau M, Owens CM, Perron MJ, Kiessling M, Autissier P, Sodroski J. 2004. The cytoplasmic body component TRIM5alpha restricts HIV-1 infection in Old World monkeys. Nature 427:848-53.
10. Goujon C, Moncorge O, Bauby H, Doyle T, Ward CC, Schaller T, Hue S, Barclay WS, Schulz R, Malim MH. 2013. Human MX2 is an interferon-induced post-entry inhibitor of HIV-1 infection. Nature 502:559-62.
11. Pornillos O, Ganser-Pornillos BK, Yeager M. 2011. Atomic-level modelling of the HIV capsid. Nature 469:424-7.
12. Ganser BK, Li S, Klishko VY, Finch JT, Sundquist WI. 1999. Assembly and analysis of conical models for the HIV-1 core. Science 283:80-3.
13. Mattei S, Glass B, Hagen WJ, Krausslich HG, Briggs JA. 2016. The structure and flexibility of conical HIV-1 capsids determined within intact virions. Science 354:1434-1437.

618 14. Yan N, Regalado-Magdos AD, Stiggelbout B, Lee-Kirsch MA, Lieberman J. 2010. The cytosolic
619 exonuclease TREX1 inhibits the innate immune response to human immunodeficiency virus
620 type 1. Nat Immunol 11:1005-13.
621 15. Jacques DA, McEwan WA, Hilditch L, Price AJ, Towers GJ, James LC. 2016. HIV-1 uses dynamic
622 capsid pores to import nucleotides and fuel encapsidated DNA synthesis. Nature 536:349-53.
623 16. Rasaiyaah J, Tan CP, Fletcher AJ, Price AJ, Blondeau C, Hilditch L, Jacques DA, Selwood DL,
624 James LC, Noursadeghi M, Towers GJ. 2013. HIV-1 evades innate immune recognition
625 through specific cofactor recruitment. Nature 503:402-405.
626 17. Yamashita M, Emerman M. 2004. Capsid is a dominant determinant of retrovirus infectivity
627 in nondividing cells. J Virol 78:5670-8.
628 18. Achuthan V, Perreira JM, Sowd GA, Puray-Chavez M, McDougall WM, Paulucci-Holthauzen A,
629 Wu X, Fadel HJ, Poeschla EM, Multani AS, Hughes SH, Sarafianos SG, Brass AL, Engelman AN.
630 2018. Capsid-CPSF6 Interaction Licenses Nuclear HIV-1 Trafficking to Sites of Viral DNA
631 Integration. Cell Host Microbe 24:392-404 e8.
632 19. Buffone C, Martinez-Lopez A, Fricke T, Opp S, Severgnini M, Cifola I, Petiti L, Frabetti S,
633 Skorupka K, Zadrozny KK, Ganser-Pornillos BK, Pornillos O, Di Nunzio F, Diaz-Griffero F. 2018.
634 Nup153 Unlocks the Nuclear Pore Complex for HIV-1 Nuclear Translocation in Nondividing
635 Cells. J Virol 92:.
636 20. Dismuke DJ, Aiken C. 2006. Evidence for a functional link between uncoating of the human
637 immunodeficiency virus type 1 core and nuclear import of the viral preintegration complex. J
638 Virol 80:3712-20.
639 21. Valle-Casuso JC, Di Nunzio F, Yang Y, Reszka N, Lienlaf M, Arhel N, Perez P, Brass AL, Diaz-
640 Griffero F. 2012. TNPO3 is required for HIV-1 replication after nuclear import but prior to
641 integration and binds the HIV-1 core. Journal of virology:JVI-00451.
642 22. Vozzolo L, Loh B, Gane PJ, Tribak M, Zhou L, Anderson I, Nyakatura E, Jenner RG, Selwood D,
643 Fassati A. 2010. Gyrase B inhibitor impairs HIV-1 replication by targeting Hsp90 and the
644 capsid protein. J Biol Chem 285:39314-28.
645 23. Zhou L, Sokolskaja E, Jolly C, James W, Cowley SA, Fassati A. 2011. Transportin 3 promotes a
646 nuclear maturation step required for efficient HIV-1 integration. PLoS Pathog 7:e1002194.
647 24. Rihn SJ, Wilson SJ, Loman NJ, Alim M, Bakker SE, Bhella D, Gifford RJ, Rixon FJ, Bieniasz PD.
648 2013. Extreme genetic fragility of the HIV-1 capsid. PLoS Pathog 9:e1003461.
649 25. Marquez CL, Lau D, Walsh J, Shah V, McGuinness C, Wong A, Aggarwal A, Parker MW,
650 Jacques DA, Turville S, Bocking T. 2018. Kinetics of HIV-1 capsid uncoating revealed by single-
651 molecule analysis. Elife 7.
652 26. Pante N, Kann M. 2002. Nuclear pore complex is able to transport macromolecules with
653 diameters of about 39 nm. Mol Biol Cell 13:425-34.
654 27. Miller MD, Farnet CM, Bushman FD. 1997. Human immunodeficiency virus type 1
655 preintegration complexes: studies of organization and composition. J Virol 71:5382-90.
656 28. Chen NY, Zhou L, Gane PJ, Opp S, Ball NJ, Nicastro G, Zufferey M, Buffone C, Luban J, Selwood
657 D, Diaz-Griffero F, Taylor I, Fassati A. 2016. HIV-1 capsid is involved in post-nuclear entry
658 steps. Retrovirology 13:28.
659 29. Bejarano DA, Peng K, Laketa V, Borner K, Jost KL, Lucic B, Glass B, Lusic M, Muller B,
660 Krausslich HG. 2019. HIV-1 nuclear import in macrophages is regulated by CPSF6-capsid
661 interactions at the nuclear pore complex. Elife 8.
662 30. Chin CR, Perreira JM, Savidis G, Portmann JM, Aker AM, Feeley EM, Smith MC, Brass AL.
663 2015. Direct Visualization of HIV-1 Replication Intermediates Shows that Capsid and CPSF6
664 Modulate HIV-1 Intra-nuclear Invasion and Integration. Cell Rep 13:1717-31.
665 31. Peng K, Muranyi W, Glass B, Laketa V, Yant SR, Tsai L, Cihlar T, Muller B, Krausslich HG. 2014.
666 Quantitative microscopy of functional HIV post-entry complexes reveals association of
667 replication with the viral capsid. Elife 3:e04114.
668 32. Hulme AE, Perez O, Hope TJ. 2011. Complementary assays reveal a relationship between HIV-
669 1 uncoating and reverse transcription. Proc Natl Acad Sci U S A 108:9975-80.

670 33. Zurnic Bonisch I, Dirix L, Lemmens V, Borrenberghs D, De Wit F, Vernaillen F, Rocha S, Christ
671 F, Hendrix J, Hofkens J, Debyser Z. 2020. Capsid labelled HIV to investigate the role of capsid
672 during nuclear import and integration. J Virol doi:10.1128/JVI.01024-19.
673 34. Mamede JI, Cianci GC, Anderson MR, Hope TJ. 2017. Early cytoplasmic uncoating is
674 associated with infectivity of HIV-1. Proc Natl Acad Sci U S A 114:E7169-E7178.
675 35. Burdick RC, Delviks-Frankenberry KA, Chen J, Janaka SK, Sastri J, Hu WS, Pathak VK. 2017.
676 Dynamics and regulation of nuclear import and nuclear movements of HIV-1 complexes. PLoS
677 Pathog 13:e1006570.
678 36. Francis AC, Marin M, Shi J, Aiken C, Melikyan GB. 2016. Time-Resolved Imaging of Single HIV-
679 1 Uncoating In Vitro and in Living Cells. PLoS Pathog 12:e1005709.
680 37. Francis AC, Melikyan GB. 2018. Live-Cell Imaging of Early Steps of Single HIV-1 Infection.
681 Viruses 10.
682 38. Francis AC, Melikyan GB. 2018. Single HIV-1 Imaging Reveals Progression of Infection through
683 CA-Dependent Steps of Docking at the Nuclear Pore, Uncoating, and Nuclear Transport. Cell
684 Host Microbe 23:536-548 e6.
685 39. Yant SR, Mulato A, Hansen D, Tse WC, Niedziela-Majka A, Zhang JR, Stepan GJ, Jin D, Wong
686 MH, Perreira JM, Singer E, Papalia GA, Hu EY, Zheng J, Lu B, Schroeder SD, Chou K, Ahmadyar
687 S, Liclican A, Yu H, Novikov N, Paoli E, Gonik D, Ram RR, Hung M, McDougall WM, Brass AL,
688 Sundquist WI, Cihlar T, Link JO. 2019. A highly potent long-acting small-molecule HIV-1 capsid
689 inhibitor with efficacy in a humanized mouse model. Nat Med 25:1377-1384.
690 40. Narayan K, Danielson CM, Lagarec K, Lowekamp BC, Coffman P, Laquerre A, Phaneuf MW,
691 Hope TJ, Subramaniam S. 2014. Multi-resolution correlative focused ion beam scanning
692 electron microscopy: applications to cell biology. J Struct Biol 185:278-84.
693 41. Petit C, Schwartz O, Mammano F. 2000. The karyophilic properties of human
694 immunodeficiency virus type 1 integrase are not required for nuclear import of proviral DNA.
695 J Virol 74:7119-26.
696 42. Price AJ, Jacques DA, McEwan WA, Fletcher AJ, Essig S, Chin JW, Halambage UD, Aiken C,
697 James LC. 2014. Host cofactors and pharmacologic ligands share an essential interface in HIV-
698 1 capsid that is lost upon disassembly. PLoS Pathog 10:e1004459.
699 43. Sowd GA, Serrao E, Wang H, Wang W, Fadel HJ, Poeschla EM, Engelman AN. 2016. A critical
700 role for alternative polyadenylation factor CPSF6 in targeting HIV-1 integration to
701 transcriptionally active chromatin. Proc Natl Acad Sci U S A 113:E1054-63.
702 44. Saito A, Ferhadian D, Sowd GA, Serrao E, Shi J, Halambage UD, Teng S, Soto J, Siddiqui MA,
703 Engelman AN, Aiken C, Yamashita M. 2016. Roles of Capsid-Interacting Host Factors in
704 Multimodal Inhibition of HIV-1 by PF74. J Virol 90:5808-5823.
705 45. Price AJ, Fletcher AJ, Schaller T, Elliott T, Lee K, KewalRamani VN, Chin JW, Towers GJ, James
706 LC. 2012. CPSF6 defines a conserved capsid interface that modulates HIV-1 replication. PLoS
707 Pathog 8:e1002896.
708 46. Aiken C. 1997. Pseudotyping human immunodeficiency virus type 1 (HIV-1) by the
709 glycoprotein of vesicular stomatitis virus targets HIV-1 entry to an endocytic pathway and
710 suppresses both the requirement for Nef and the sensitivity to cyclosporin A. J Virol 71:5871-
711 7.
712 47. Bos E, Hussaarts L, van Weering JR, Ellisman MH, de Wit H, Koster AJ. 2014. Vitrification of
713 Tokuyasu-style immuno-labelled sections for correlative cryo light microscopy and cryo
714 electron tomography. J Struct Biol 186:273-82.
715 48. Marini B, Kertesz-Farkas A, Ali H, Lucic B, Lisek K, Manganaro L, Pongor S, Luzzati R, Recchia
716 A, Mavilio F, Giacca M, Lusic M. 2015. Nuclear architecture dictates HIV-1 integration site
717 selection. Nature 521:227-31.
718 49. Stultz RD, Cenker JJ, McDonald D. 2017. Imaging HIV-1 Genomic DNA from Entry through
719 Productive Infection. J Virol 91.

720 50. Puray-Chavez M, Tedbury PR, Huber AD, Ukah OB, Yapo V, Liu D, Ji J, Wolf JJ, Engelman AN,
721 Sarafianos SG. 2017. Multiplex single-cell visualization of nucleic acids and protein during HIV
722 infection. Nat Commun 8:1882.
723 51. Bell P, Montaner LJ, Maul GG. 2001. Accumulation and intranuclear distribution of
724 unintegrated human immunodeficiency virus type 1 DNA. J Virol 75:7683-91.
725 52. Komatsu T, Quentin-Froignant C, Carlon-Andres I, Lagadec F, Rayne F, Ragues J, Kehlenbach
726 RH, Zhang W, Ehrhardt A, Bystricky K, Morin R, Lagarde JM, Gallardo F, Wodrich H. 2018. In
727 vivo labelling of adenovirus DNA identifies chromatin anchoring and biphasic genome
728 replication. J Virol doi:10.1128/JVI.00795-18.
729 53. Mariame B, Kappler-Gratias S, Kappler M, Balor S, Gallardo F, Bystricky K. 2018. Real-time
730 visualization and quantification of human Cytomegalovirus replication in living cells using the
731 ANCHOR DNA labeling technology. J Virol doi:10.1128/JVI.00571-18.
732 54. Graham TG, Wang X, Song D, Etson CM, van Oijen AM, Rudner DZ, Loparo JJ. 2014. ParB
733 spreading requires DNA bridging. Genes Dev 28:1228-38.
734 55. Sanchez A, Cattoni DI, Walter JC, Rech J, Parmeggiani A, Nollmann M, Bouet JY. 2015.
735 Stochastic Self-Assembly of ParB Proteins Builds the Bacterial DNA Segregation Apparatus.
736 Cell Syst 1:163-73.
737 56. de Chaumont F, Dallongeville S, Chenouard N, Herve N, Pop S, Provoost T, Meas-Yedid V,
738 Pankajakshan P, Lecomte T, Le Montagner Y, Lagache T, Dufour A, Olivo-Marin JC. 2012. Icy:
739 an open bioimage informatics platform for extended reproducible research. Nat Methods
740 9:690-6.
741 57. Paul-Gilloteaux P, Heiligenstein X, Belle M, Domart MC, Larijani B, Collinson L, Raposo G,
742 Salamero J. 2017. eC-CLEM: flexible multidimensional registration software for correlative
743 microscopies. Nat Methods 14:102-103.
744 58. Briggs JA, Simon MN, Gross I, Krausslich HG, Fuller SD, Vogt VM, Johnson MC. 2004. The
745 stoichiometry of Gag protein in HIV-1. Nat Struct Mol Biol 11:672-5.
746 59. Gu J, D'Andrea M. 1989. Comparison of detecting sensitivities of different sizes of gold
747 particles with electron-microscopic immunogold staining using atrial natriuretic peptide in
748 rat atria as a model. Am J Anat 185:264-70.
749 60. Butler SL, Hansen MS, Bushman FD. 2001. A quantitative assay for HIV DNA integration in
750 vivo. Nat Med 7:631-4.
751 61. Saad H, Gallardo F, Dalvai M, Tanguy-le-Gac N, Lane D, Bystricky K. 2014. DNA dynamics
752 during early double-strand break processing revealed by non-intrusive imaging of living cells.
753 PLoS Genet 10:e1004187.
754 62. Maldarelli F, Wu X, Su L, Simonetti FR, Shao W, Hill S, Spindler J, Ferris AL, Mellors JW,
755 Kearney MF, Coffin JM, Hughes SH. 2014. HIV latency. Specific HIV integration sites are linked
756 to clonal expansion and persistence of infected cells. Science 345:179-83.
757 63. Liu R, Simonetti FR, Ho YC. 2020. The forces driving clonal expansion of the HIV-1 latent
758 reservoir. Virol J 17:4.
759 64. Chun TW, Engel D, Berrey MM, Shea T, Corey L, Fauci AS. 1998. Early establishment of a pool
760 of latently infected, resting CD4(+) T cells during primary HIV-1 infection. Proc Natl Acad Sci U
761 S A 95:8869-73.
762 65. Charneau P, Mirambeau G, Roux P, Paulous S, Buc H, Clavel F. 1994. HIV-1 reverse
763 transcription. A termination step at the center of the genome. J Mol Biol 241:651-62.
764 66. Munch J, Rucker E, Standker L, Adermann K, Goffinet C, Schindler M, Wildum S, Chinnadurai
765 R, Rajan D, Specht A, Gimenez-Gallego G, Sanchez PC, Fowler DM, Koulov A, Kelly JW,
766 Mothes W, Grivel JC, Margolis L, Keppler OT, Forssmann WG, Kirchhoff F. 2007. Semen-
767 derived amyloid fibrils drastically enhance HIV infection. Cell 131:1059-71.
768 67. Yolamanova M, Meier C, Shaytan AK, Vas V, Bertoncini CW, Arnold F, Zirafi O, Usmani SM,
769 Muller JA, Sauter D, Goffinet C, Palesch D, Walther P, Roan NR, Geiger H, Lunov O, Simmet T,
770 Bohne J, Schrezenmeier H, Schwarz K, Standker L, Forssmann WG, Salvatella X, Khalatur PG,
771 Khokhlov AR, Knowles TP, Weil T, Kirchhoff F, Munch J. 2013. Peptide nanofibrils boost

retroviral gene transfer and provide a rapid means for concentrating viruses. Nat Nanotechnol 8:130-6.
68. Slot JW, Geuze HJ. 2007. Cryosectioning and immunolabeling. Nat Protoc 2:2480-91.
69. Mastronarde DN. 2005. Automated electron microscope tomography using robust prediction of specimen movements. J Struct Biol 152:36-51.
70. Kremer JR, Mastronarde DN, McIntosh JR. 1996. Computer visualization of three-dimensional image data using IMOD. J Struct Biol 116:71-6.
71. Forster B, Van De Ville D, Berent J, Sage D, Unser M. 2004. Complex wavelets for extended depth-of-field: a new method for the fusion of multichannel microscopy images. Microsc Res Tech 65:33-42.
72. Thevenaz P, Unser M. 2007. User-friendly semiautomated assembly of accurate image mosaics in microscopy. Microsc Res Tech 70:135-46.

Legends

FIG. 1 Viral reverse transcription correlates with HIV-1 CA and IN association. **(**A) Comparison of the infectivity of HIV-1 carrying the IN wild type or the IN fused to HA tag analysed by beta-galactosidase assay, normalized by amount of proteins. HeLa cells (10^6 cells) infected with 500ng of p24 of HIV-1ΔEnv IN_{HA} / VSV-G fixed at 6 h post infection and labelled with antibodies anti-p24 (green) and anti-HA (red), host DNA is labelled by Hoechst (blue). Analysis of the percentage of IN/CA co-localization analysed by Image J and by Graph Pad Prism 7. (B) HeLa cells infected for 24 h in presence or not of the drug PF74 at low dose (1.25 µM) or high dose (10 µM). Cells were fixed on 4% of PFA and labelled with antibodies anti p24, anti-HA and anti-Nup153. Co-localization between CA and IN was analysed by ImageJ and by Graph Pad Prism 7. (C) DNA synthesis has been evaluated by qPCR through the amplification of late reverse transcripts (LRT). The infectivity was analysed at 48 h post infection by beta galactosidase assay and normalized by protein amount. (D) Effect of PF74 doses on HIV-1 CA and IN detections at 6 h post infection in HeLaP4R5 cells by confocal microscopy. (E) Analysis of the percentage of IN/CA co-localization by Image J and by Graph Pad Prism 7 (graph on the top right). The level of infectivity has been evaluated at 48h post infection by beta galactosidase assay normalized for the quantity of proteins as reported in the histogram on the bottom right.

Differences were considered statistically significant at a P value of <0.0001 (****), <0.001 (***), or <0.01 (**), or <0.1 (*), analysed by Graph Pad Prism 7 (*T student test*).

FIG. 2 The road of viral CA complexes before and after nuclear translocation (A) Images of HIV-1 virions englobed in the endosomes or cores escaping from the endosomes obtained by TEM. First from the left a 2D plane extracted from the tomogram of the endosomes containing viral particles, on the right the cell volume reconstructed and coloured (red for the

envelope, blue for the cores, yellow for the borders of the endosome and green for the nuclear membrane). (B) Examples of structures resembling "core like structures" docked at the NPC by TEM. A negative control based on uninfected cells is shown in panel i. Panels ii and iii show "core like structures" docked at the NPC detected by 2 CA gold 10nm particles revealing the antibodies anti-p24 (NIH183-H12-5C) attached. Panels iv and v show intranuclear CA complexes. Scale Bar 100nm. Schema of the labelling method, first Ab anti CA and secondary Ab conjugated to gold particles. Quantification analysis of the CA gold particles distribution in viral complexes (~ 42) located in the cytoplasm or in the nucleus. The percentage of CA complexes detected by 2 CA gold particles associated or not to a "core like shape" and 3CA gold particles detected in the cytoplasm or in the nucleus. (C) HeLaP4R5 cells infected with HIV-1 IN_{HA} / VSVG. The sections were prepared and immunolabelled as in panel B, using a primary antibody anti CA (AG3.0). Black arrows indicate gold particles of 10 nm conjugated to a secondary Ab. Scale Bar 200nm. (D) HeLa P4R5 cells infected with HIV-1 IN_{HA} carrying on the WT envelope. The sections were prepared and immunolabelled as in panel B. The areas containing the viral CA complexes are enlarged in squares on the upper right of the pictures. Scale Bar 100nm. (E) Schema of the labelling method, first Ab anti CA and protein A gold. Cryo-electron and immunogold labelling have been used. The image contains several CA complexes (pointed out by black arrows) each one with multiple CA proteins showed by gold particles. The magnified views of the areas enclosed by black rectangles display the differences in the gold distribution between outside and inside the nucleus. Images were obtained using an antibody against HIV-1 CA followed by incubation with protein A coupled to 10nm gold. Tomogram of a representative intranuclear CA complex highlighted with black rectangle. Sections were imaged in a T12 FEI electron microscope with tomography capabilities. The tomogram of the cell volume was reconstructed and manually segmented using IMOD. The upper panels, showing a larger view of the cell, starting from the left contain several planes (number 31, 43 and 49 out of 91 total slices) of the tomogram and the segmentation obtained from the reconstructed tomographic cell volume containing the gold labelled CA complexes, nuclear envelope (NE), endoplasmic reticulum (ER) and mitochondria (yellow, green, magenta and purple respectively). On the bottom is depicted the magnified views of the areas delimited by dashed lines on the upper panels.

FIG. 3 CA protein multimers are associated to IN inside the host nucleus. (A) Some CA complexes detected at 6 h post infection contain IN. The double labelling gold against

845 primary antibodies anti-p24 (10nm) and anti-HA (to label IN) (6nm) highlights the
846 association of both proteins particularly inside the nucleus of HeLa cells. CA/IN association
847 in the cytoplasm (~41%) and in the nucleus (~58%) has been calculated and represented in the
848 graph on the right. B**)** Primary $CD4^+$ T cells were isolated from healthy donors and infected
849 with 4000ng of p24 of HIV-1. Comparison of the infectivity in primary $CD4^+$ T cells
850 (calculated as % of positive p24 cells analysed by cytofluorimetry) between wild type
851 enveloped viruses carrying on the wild type IN or the IN fused to HA tag. C) $CD4^+$ T cells
852 were challenged with HIV-1 IN_{HA} / VSVG and samples were processed for immunoelectron
853 microscopy after 9 hours from infection and stained with antibodies against capsid and HA
854 for the integrase. Magnified insets represent: i) 2CA gold complexes located in the
855 cytoplasmic area ii) and iii) 3CA complexes containing integrase as well. The black arrows
856 correspond to capsid labelled with 10nm gold, the white arrows point the integrase labelled
857 with 6nm gold. D) Analysis of the % CA gold forms in the cytoplasm (cy) vs the nucleus (nu)
858 containing 2CA gold or 3CA gold particles, respectively.
859
860 FIG. 4: Detection of the retrotranscribed HIV-1 DNA in infected cells. (A) Schema of the
861 HIV-1 ANCHOR system based on lentiviral vectors carrying on the OR-GFP cDNA under
862 the control of CMV promoter (LV OR-GFP) and HIV-1 containing the ANCH3, target
863 sequence of OR proteins (HIV-1ΔEnvIN_{HA}ΔNefANCH3/VSV-G). (B) HeLa P4R5 cells were
864 transduced with LV OR-GFP. The efficiency of OR-GFP expression was monitored by
865 western blotting using antibody against GFP. As a loading control, samples were also blotted
866 using antibody against actin. HeLa cells stably expressing OR-GFP infected or not with HIV-
867 1ΔEnvIN_{HA}ΔNef ANCH3/VSV-G (MOI 50) have been imaged by fluorescence microscopy
868 at 24h post infection using water immersion objective in epifluorescence. The number of
869 proviruses has been detected by ALU/PCR on HeLa P4R5 ORGFP infected with HIV-1 or
870 HIV-1 ANCH3.
871
872 FIG. 5 Specificity of HIV-1 ANCHOR system to detect the retrotranscribed DNA. (A)
873 HeLaP4R5 cells stably transduced with LVOR-GFP were infected at different MOIs of HIV-
874 1 ANCH3 and imaged after 24 h by confocal microscopy. Nuclear viral DNA spots per single
875 GFP+ cell were analysed in 2D by ImageJ. Correlation analysis and the Pearson's coefficient
876 as well as statistical analysis have been performed by Graph Pad Prism 7 (Anova test). (B)
877 HeLaP4R5 cells infected at MOI 50 with HIV-1ΔEnvIN_{HA}ΔNef ANCH3/VSV-G in presence
878 or not of PF74 (low dose, 1.25μM; high dose 10 μM). Cells were imaged by confocal

879 microscope at 24h post-infection. (C) Individual spots inside the nuclei were manually
880 counted and statistically analysed in 2D by Graph Pad Prism 7, statistics were calculated
881 using two-tailed Student's t test, P value <0.0001 (****) and nonsignificant (ns). (D) Viral
882 nuclear import has been evaluated by qPCR (2LTRs) and normalized by actin. Statistical
883 analysis has been calculated by Graph Pad Prism 7 using two-tailed Student's t test.
884 Differences were considered statistically significant at a P value of <0.001 (***), or <0.01
885 (**).(E) Confocal microscopy of intranuclear spots detections in HeLa P4R5 OR-GFP
886 challenged with MOI30 of HIV-1 ANCH3 in presence or not of NEV at 24h post-infection.
887 2D statistical analysis of a manual count of intranuclear spots has been performed by Graph
888 Pad Prism 7. All data are representative of two or more independent experiments.
889
890 FIG. 6 Multiple CA proteins leading retrotranscribed DNA detected by CLEM. (A) HeLa
891 P4R5 transduced with OR-GFP were infected with HIV-1 ANCH3 and processed for
892 correlative light and electron microscopy (CLEM). To achieve a precision correlation,
893 fluorescent beads of 200nm were added, visible also by EM. CLEM results on HeLa P4R5
894 OR-GFP cells at 6 h p.i. show the GFP signal in green revealing the location of HIV-1 DNA.
895 The signal of OR-GFP is amplified by using an antibody against GFP. HIV-1 CA is detected
896 by a first antibody anti-CA and a secondary antibody gold conjugated (gold 10nm). The
897 yellow signals correspond to the beads emitting in green and in red channels. On the top
898 right, the magnified view of the black square is shown. The green signal shows the location of
899 viral DNA, associated to the CA gold labels, dark dots. (B) Another biological replicate of
900 CLEM shows multimer of CA proteins (dark dots) shrouding the vDNA (green signal) during
901 nuclear translocation (panel on the left). Panel on the right shows an example of the precision
902 correlation process applied. The precision of the correlation between TEM and fluorescence
903 images were estimated with ec-CLEM plugin under the icy environment. The calibration bar
904 represents the precision achieved in nm by the different area of the cells. The dashed circle
905 shows the area enlarged in the black box of the panel on the left.
906
907 FIG. 7 Viral complexes composed by CA and retrotranscribed DNA near the NE and inside
908 the nucleus. (A) Double gold labelling coupled to TEM show CA / OR-GFP (viral DNA) as
909 part of the same complex near the NE. Viral DNA is detected by the presence of clusters
910 formed by multiple OR-GFP bound to ANCH3 sequence cloned in HIV-1 genome. OR-GFP
911 proteins are labelled by the same primary antibody against GFP used in CLEM and a
912 secondary antibody conjugated with gold particles of 5nm. HIV-1 CA is revealed by a

913 primary antibody against CA (NIH183-H12-5C) and a secondary antibody conjugated with
914 gold (10nm). Scale bars 100nm. (B) Intranuclear viral complexes contain CA and viral DNA
915 detected by double gold labelling coupled to TEM. Scale bar 100 nm.
916
917

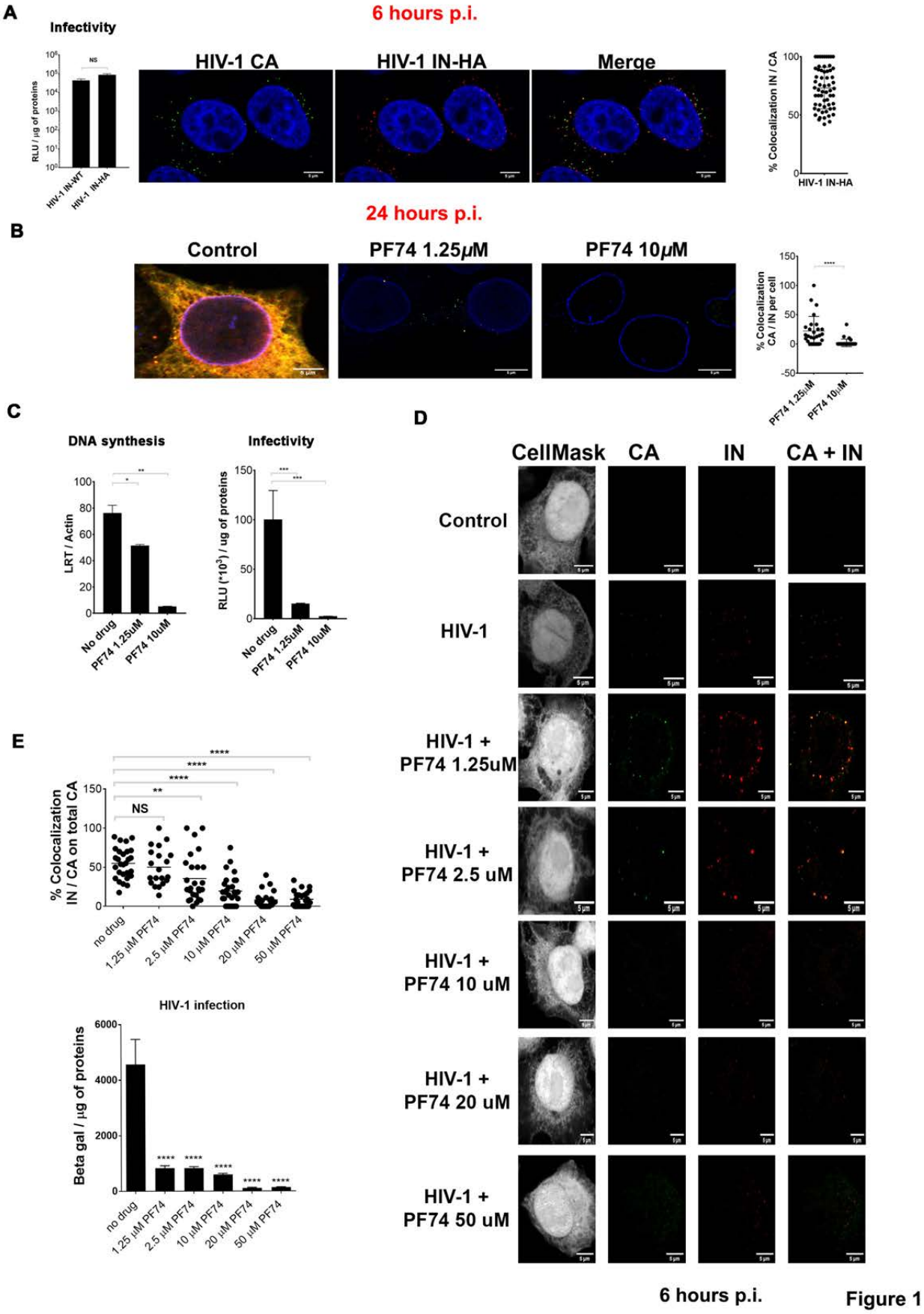

Figure 1

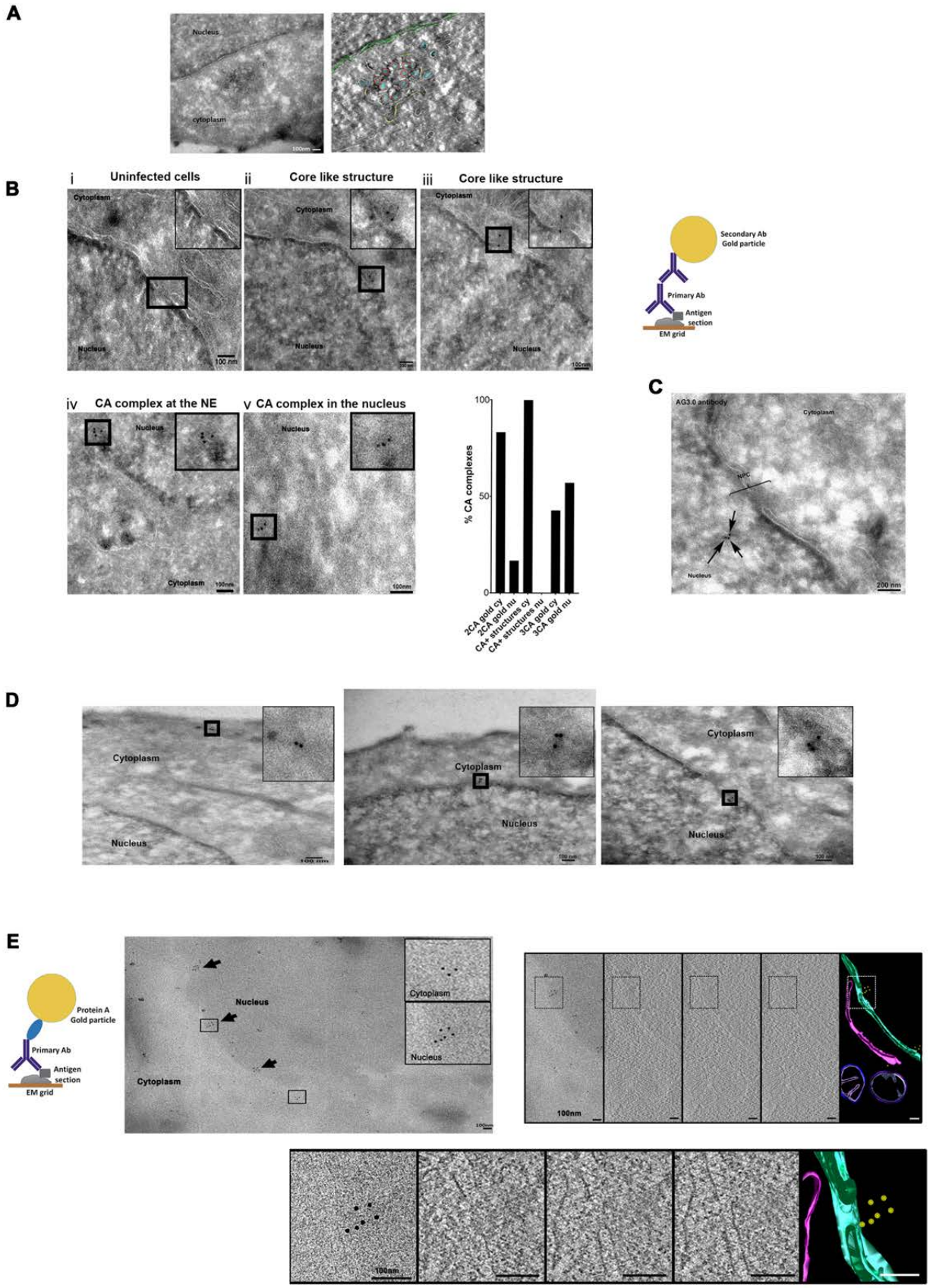

Figure 2

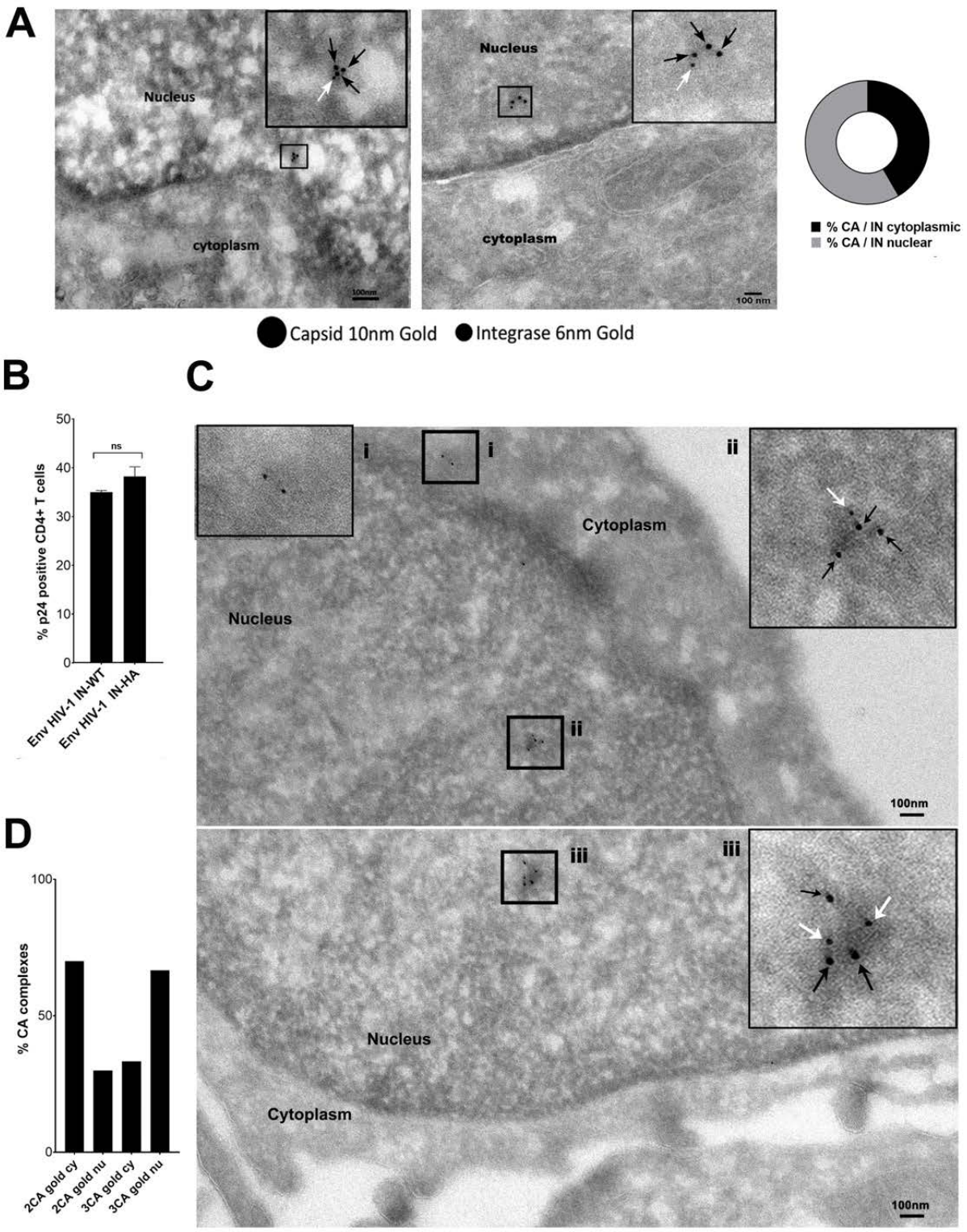

Figure 3

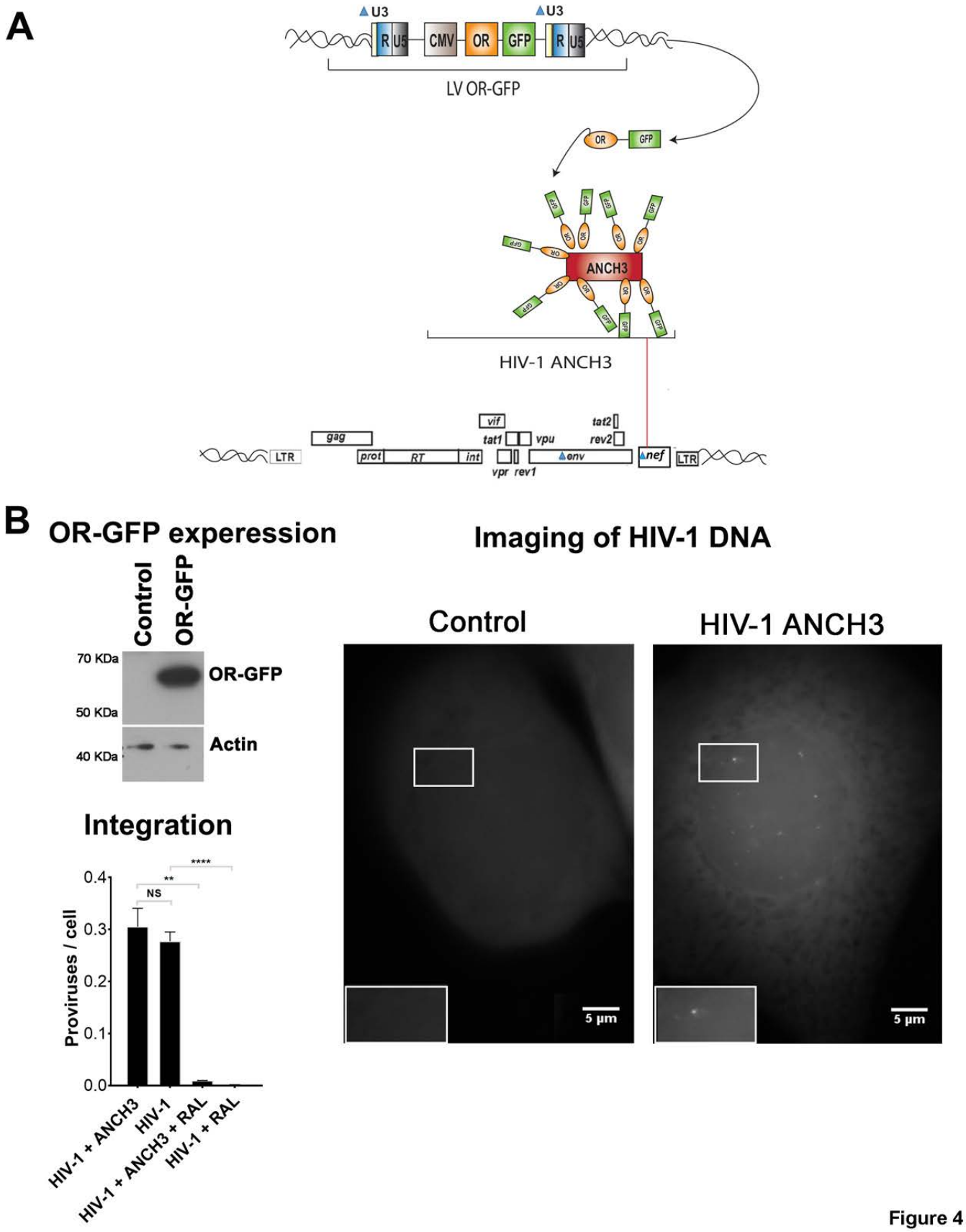

Figure 4

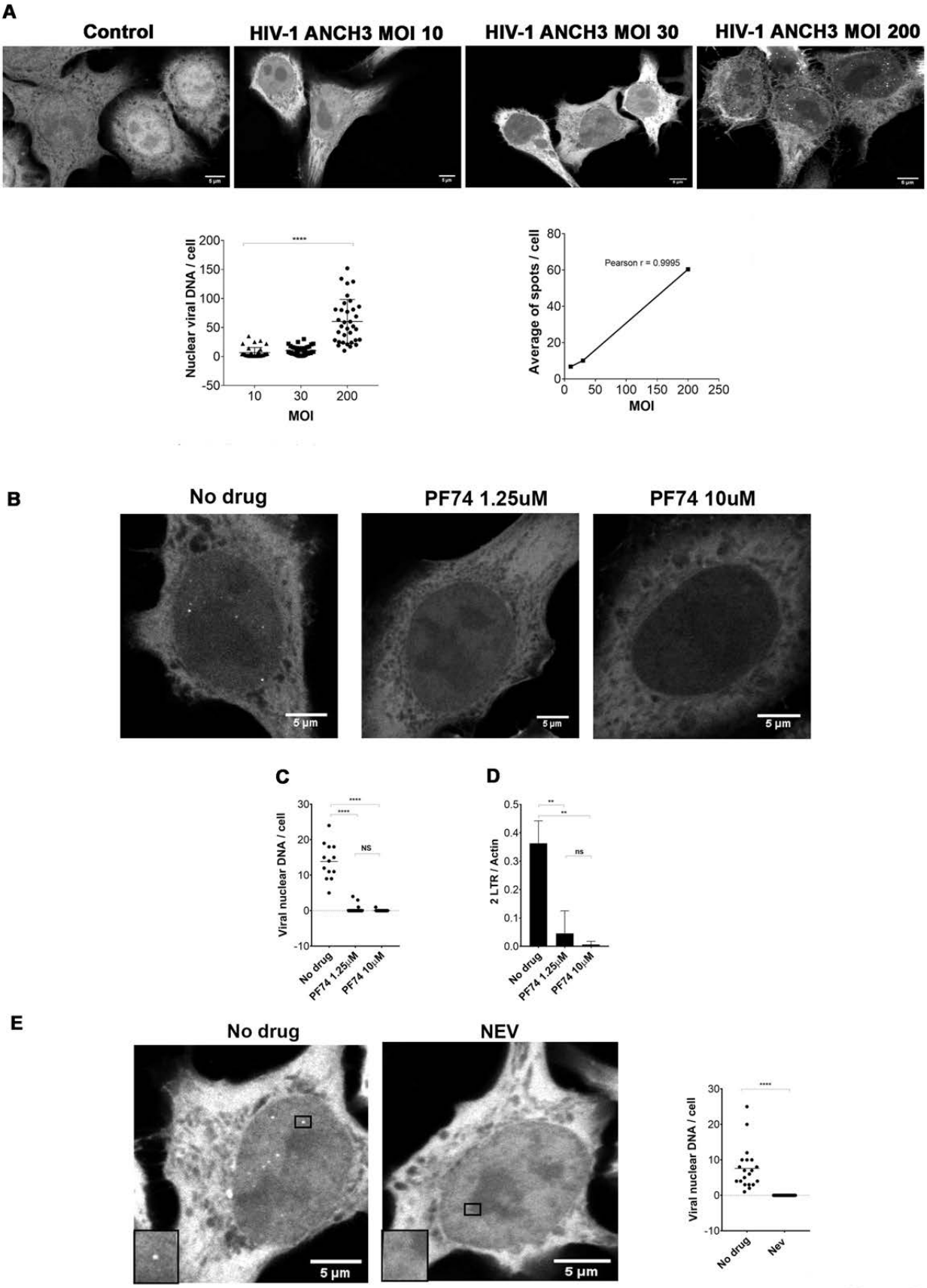

Figure 5

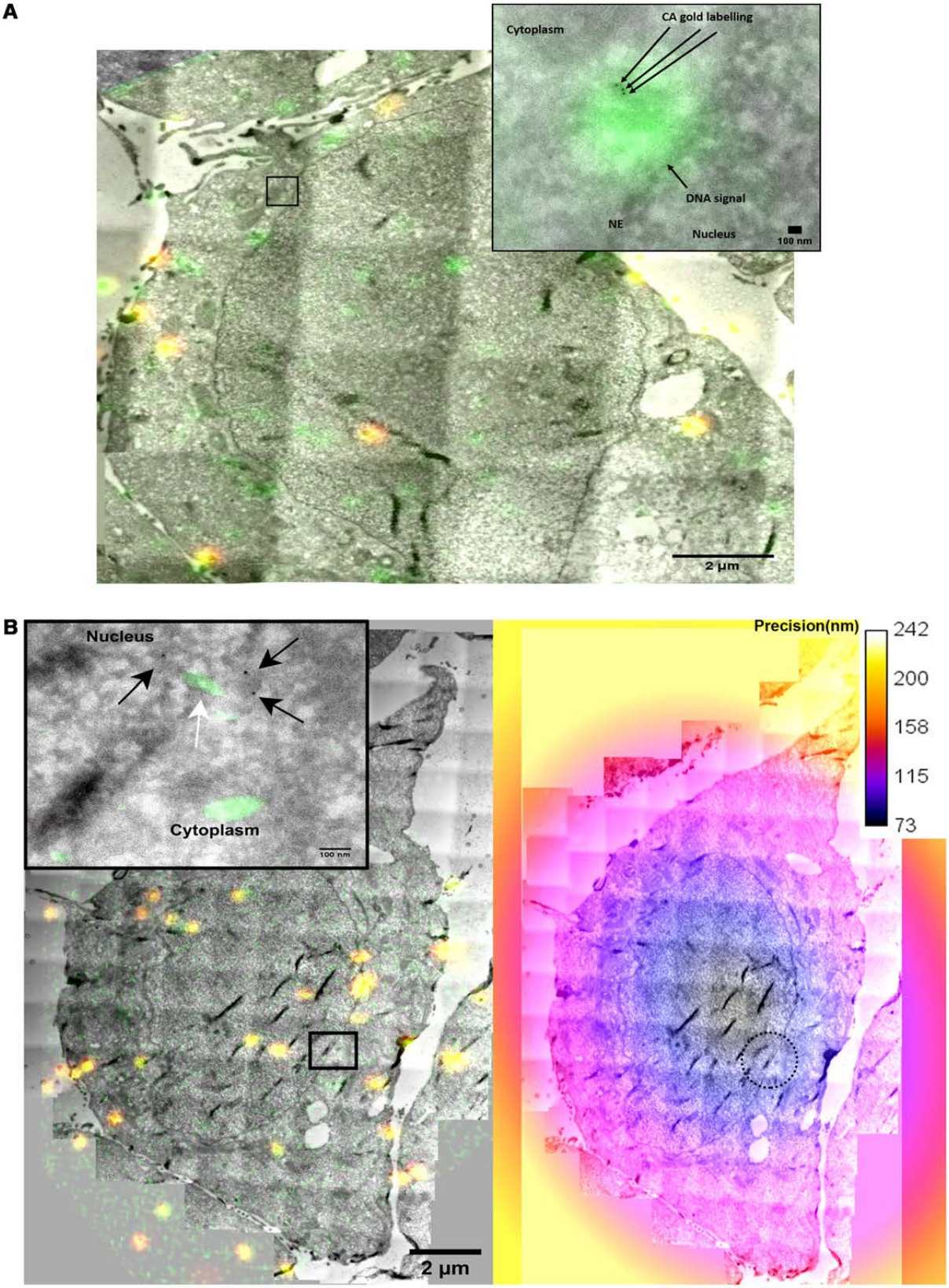

Figure 6

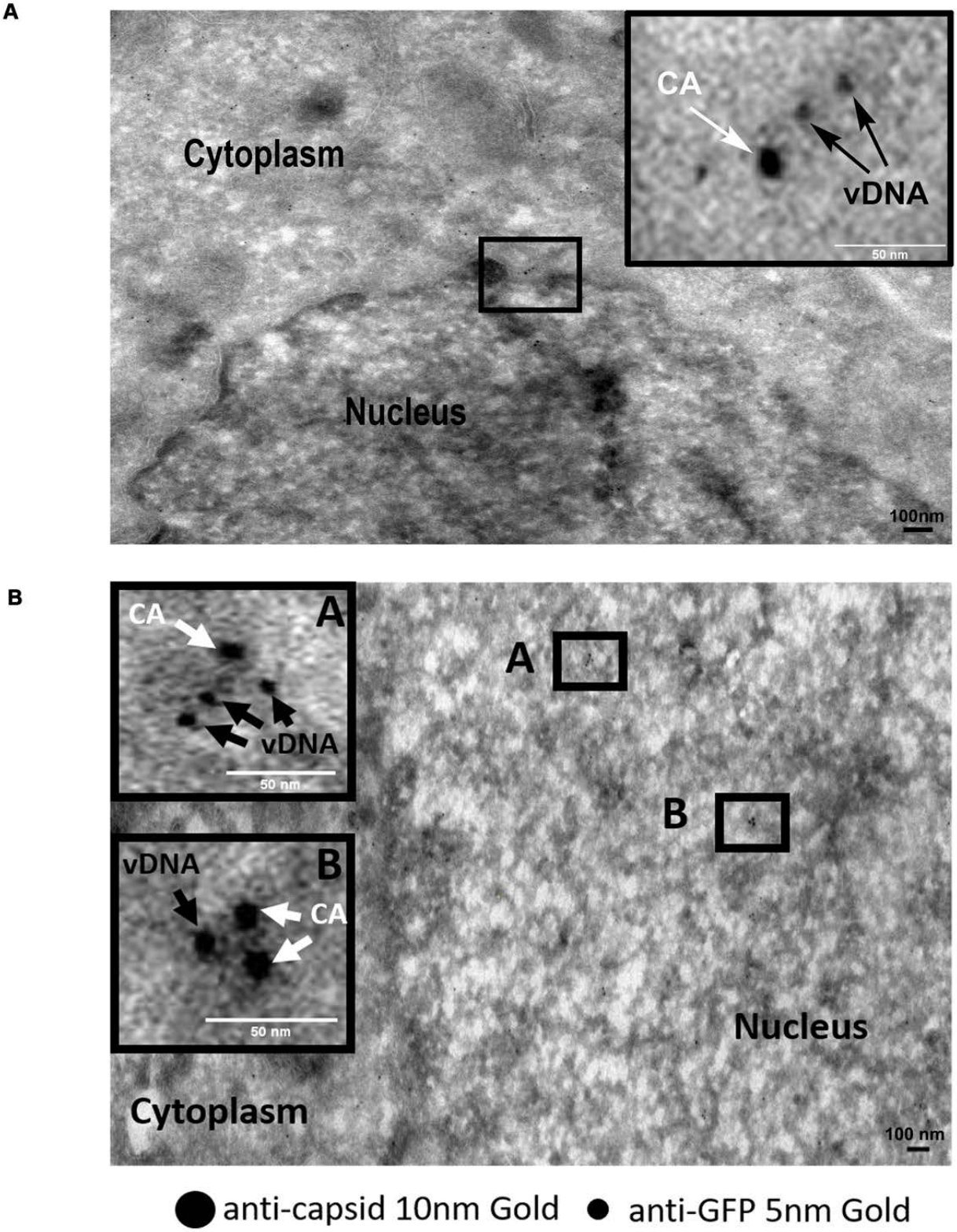

Figure 7